# The Design of AC Permanent Magnet Motors for Electric Vehicles: A Design Methodology

James Goss, Rafal Wrobel, Phil Mellor, Dave Staton

***Abstract*—this paper presents a complete methodology for the design of AC permanent magnet motors for electric vehicle traction. Electromagnetic, thermal and mechanical performance aspects are considered and modern CAD tools are utilised throughout the methodology. A 36 slot 10 pole interior permanent magnet design example is used throughout the analysis.**

***Index Terms*— Design Methodology, Permanent Magnet Motor, Traction, Computer-Aided Design**

## I. INTRODUCTION

For an engineer using computer aided design (CAD) tools to design a permanent magnet (PM) motor for a traction application there is little guidance available. A small amount of academic literature exists discussing design methodologies, these are typically incomplete and generally take the form of either an objective analytical calculation or an optimisation problem, describing the derivation of some motor parameters for a well-defined problem that is difficult to generalise to different design tasks [1], [2],[3], [4]. In this literature CAD tools are typically primarily used either to validate the result of analytical sizing exercises or as a black box optimisation engine. Alternatively some literature exists relating to the use of CAD tools [5] in a design process, this advocates an unstructured trial and error approach. This is clearly at odds with the structured deductive design philosophy proposed in academic literature and is likely to result in a satisfactory rather than optimal design. Here a methodology is presented that attempts to reconcile these approaches, adopting the structured scientific approach to design found in academia while utilising a number of CAD tools and remaining flexible enough to be used across a variety of design projects. The aim of this paper is to present a complete methodology that provides a simple, rigorous and scientific approach to the design of AC PM electric motors for traction applications utilising a number of modern CAD design tools where electromagnetic, thermal and mechanical performance aspects are taken into account. The methodology aims to optimise performance across the entire operational envelope and the techniques detailed in [6] are used throughout to achieve this.

This work was supported by the Bristol University EPSRC funded Industrial Doctorate Centre in Systems (Grant EP/G037353/1) and Motor Design Ltd.
J.Goss and D.Staton are with Motor Design Ltd, UK, (e-mail j.goss@motor-design.com and d.staton@motor-design.com)
R.Wrobel and P.Mellor are with The University of Bristol, Electronic and Electrical Engineering Department, UK, (e-mail r.wrobel@bristol.ac.uk and p.h.mellor@bristol.ac.uk)

It is understood that electric motor design is not simply an objective calculation and as such the methodology allows flexibility to accommodate for the intuition and experience of the design engineer, as well as constraints or goals that cannot simply be expressed within the technical specification. Throughout this paper the methodology is illustrated using examples from the design of a 36 slot 10 pole interior permanent magnet motor for a small electric vehicle application. The software tools utilised throughout this procedure are SPEED PC-BDC and PC-FEA [7] for electromagnetic modelling, Motor-CAD [8] for thermal modelling, Autodesk inventor [9] for mechanical modelling and Motor-LAB [10] to analyse the thermal and electromagnetic performance of the design across the full operating envelope.

## II. OVERVIEW OF THE DESIGN METHODOLOGY

Fig. 1 shows a basic outline of the methodology, no iterative loops are shown as these are dependent on the specific design, however some iteration will be required and it should be minimised where possible.

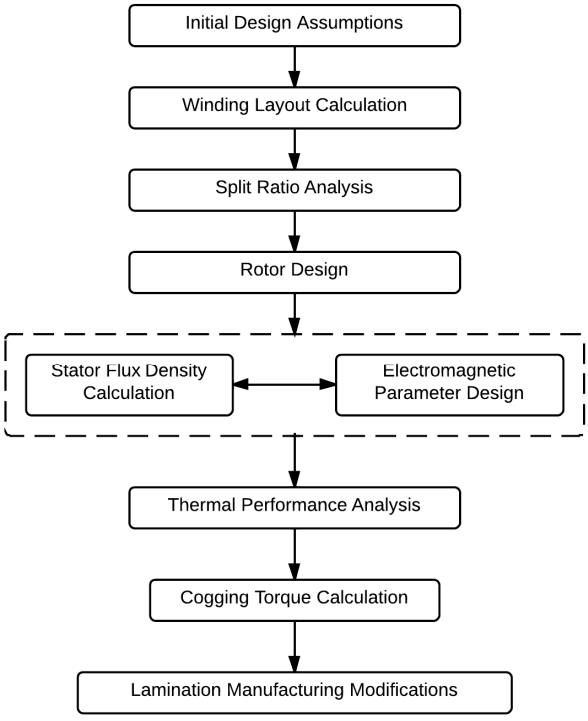


Figure 1- Overview of the design methodology

Initially a number of parameters are set as is typical in most design projects. In the given example these are the slot/pole combination, 36 slot 10 pole, the stator outer radius, 87.5mm, the machine topology, radial flux inner rotor interior permanent magnet and the choice of materials, N38EH NeFeB magnets and M300-35A electrical steel. The winding layout is then calculated using the method given in [11]. The split ratio task deduces the ratio of the stator outer diameter to stator bore that gives the minimum amount of copper loss when rated torque is produced. Next the rotor lamination is designed to maximise the airgap flux density of the motor for a maximum specified mechanical safety factor at full speed. The stator flux density is chosen such that the combined copper and iron losses are minimised across the full speed range of the motor and the electromagnetic parameters are chosen to optimise the torque/speed characteristics of the motor against the specified driving cycles. This is achieved by modifying the number of turns and the motors active length. The slot and tooth shapes are then computed using a genetic algorithm that aims to maximise torque for a fixed value of copper loss. Next lumped parameter thermal modelling is used to compute the thermal envelope of the design and model the temperatures over a worst-case driving cycle, allowing the engineer to evaluate the cooling requirements that enable the design to achieve the specified continuous and peak performance. The cogging torque is then calculated and design modifications made where necessary. Finally, the lamination design is given the alignment features required during the manufacturing and assembly process.

## III. SPLIT RATIO ANALYSIS

The split ratio is the ratio of the stator bore to the stator outer diameter. As the rotor radius is increased the motor is able to produce the same torque with reduced winding current, however when constrained by a fixed outer diameter the slot area is consequently decreased, increasing the winding resistance and hence reducing the maximum thermally constrained operating current. Here we aim to discover the value of the split ratio that maximises the ratio of torque to copper loss. A number of designs are generated with a set magnetic loading, 0.65T and core flux density, 1.2T to ensure a fair comparison. This is achieved by scripting an electromagnetic FEA design tool and solving for the specified flux densities using a similar approach to [12]. At this stage the specific rotor design is not critical. From here, the copper loss associated with an arbitrary torque value, 20Nm in this example, at a low speed maximum torque/amp (MTPA) operating point is calculated for each design. From fig. 2, it can be seen that the minimum copper loss occurs at a value of 0.54, however, in this example the gradient of the graph is small between 0.5 and 0.55, and hence any value between these would be acceptable.

A number of other considerations are demonstrated in table I, the lower split ratio designs require slightly less magnet material to achieve the same magnetic loading and the slot depth is greater which may improve heat transfer through the slot. However the short circuit current increases with split ratio which will improve the peak electromagnetic power of the design at high speeds. In addition the current rating falls with increasing split ratio giving a reduced maximum inverter VA rating requirement. As the design develops throughout the methodology this stage should be re-visited to evaluate if the chosen value of split ratio is still close to the optimum.

TABLE I
SPLIT RATIO ANALYSIS RESULTS

| *Split Ratio* | *0.5* | *0.52* | *0.54* | *0.56* | *0.58* | *0.6* |
|---|---|---|---|---|---|---|
| Phase Resistance (mΩ) | 4.8 | 5.1 | 5.4 | 5.9 | 6.3 | 6.8 |
| Magnet Length (mm) | 20.7 | 20.8 | 20.9 | 21.1 | 21.2 | 21.4 |
| Slot Depth (mm) | 37.3 | 35.4 | 33.5 | 31.6 | 29.8 | 27.9 |
| $I_{sc}$ (A) | 142 | 147 | 154 | 160 | 169 | 173 |
| Saliency Ratio | 1.57 | 1.59 | 1.61 | 1.63 | 1.67 | 1.69 |
| $I_s$ (A) | 68.4 | 66.2 | 64.0 | 62.0 | 60.5 | 59.0 |
| Gamma for MTPA (°) | 14 | 13.7 | 13.2 | 12.9 | 12.7 | 12.4 |
| Copper Loss (W) | 75.5 | 75.3 | 75.1 | 76.0 | 77.5 | 79.9 |

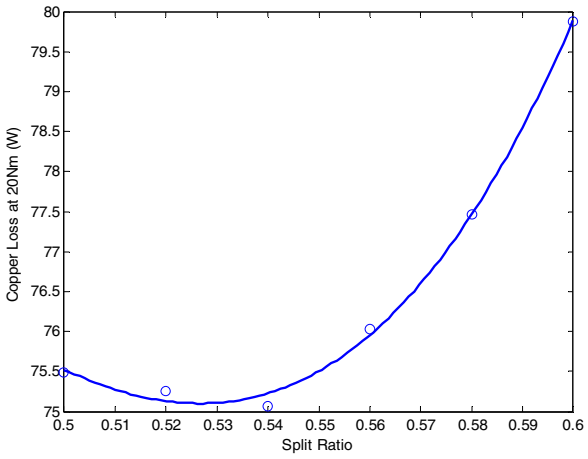


Figure 2- Variation of Copper Loss at 20Nm with Split Ratio

## IV. ROTOR DESIGN

A given magnet volume can be utilised differently, depending on the dimensions set for the magnet, this affects both the peak airgap flux density, often described as the magnetic loading and the saliency, $L_q/L_d$, of the rotor. Maximising the magnetic loading for a given magnet volume ensures that the magnet is being used most effectively. A larger value of saliency is desirable as this also improves the motors torque density. The rotor topology used as an example here is a single pole piece rectangular interior magnet arrangement however the principles can be adapted to suit v-shaped or multi-layer magnet arrangements. The dimensions used throughout this analysis are detailed in fig. 3.

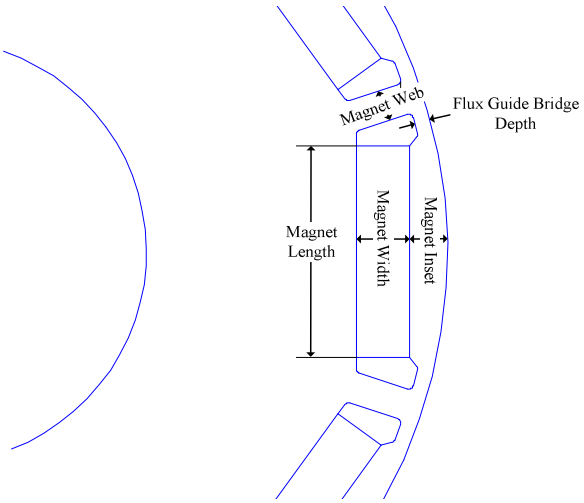


Figure 3-Magnet and Flux Guide Dimensions

### A. *Magnet Length*

The variation in magnetic loading and saliency ratio with different magnet lengths can be investigated using electromagnetic FEA.

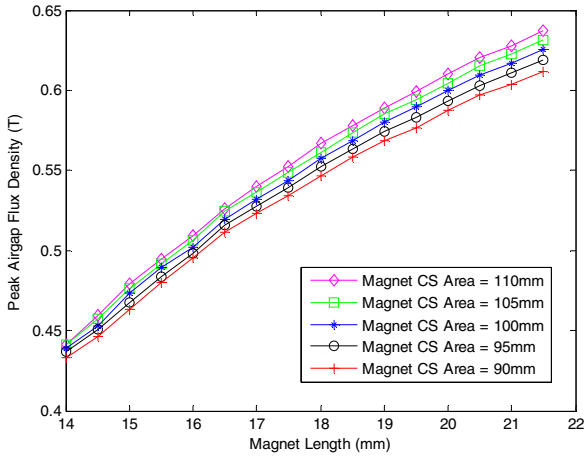


Figure 4 -Variation of Airgap Flux Density with Magnet Length

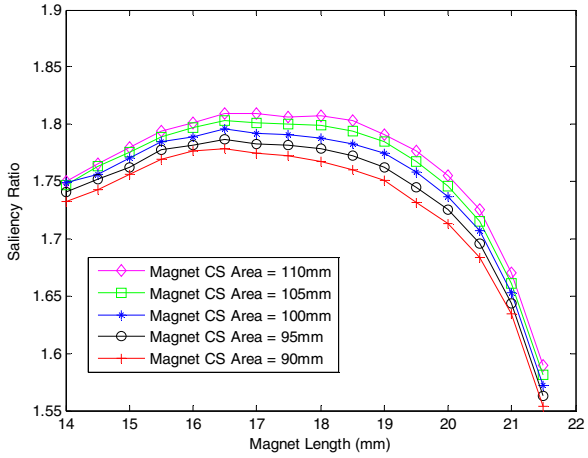


Figure 5-Variation of Saliency Ratio with Magnet Length

Figs. 4-5 demonstrate the effect increasing magnet length, with a fixed magnet cross-sectional area, has on the magnetic loading and saliency ratio. For all magnet areas the magnetic loading increases almost linearly with length while the saliency ratio peaks at a particular length before falling rapidly. This is largely unaffected by the choice of cross sectional magnet area, therefore the optimum magnet length can be chosen at this stage. In this example a length of 20.5mm maximises the airgap flux density without significantly impacting the saliency ratio.

### B. *Magnet Width*

The magnetic loading improves as the magnet is moved closer to the airgap resulting in a reduced inset and bridge depth however too small and the centrifugal forces on the rotor at high rotational speeds will cause mechanical failure. Here the magnet width that maximises the magnetic loading for a given mechanical stress safety factor is found. Five rotors have been analysed with a magnet width ranging from 3 to 7mm. All have been designed using an automated procedure which varies the magnet and flux guide position from the rotor circumference to solve for a magnetic loading of 0.65T. The mechanical safety factor is then analysed using a mechanical FEA stress analysis tool at 10,000rpm, the dimensions and results for the five rotors are given table II. The minimum stress and hence highest safety factor occurs at a magnet length of 5mm. Therefore a value close to this maximises the magnetic loading for a given safety factor.

TABLE II
MAGNET WIDTH ANALYSIS

| *Magnet Width (mm)* | *3* | *4* | *5* | *6* | *7* |
|---|---|---|---|---|---|
| Magnet Length (mm) | 20.5 | 20.5 | 20.5 | 20.5 | 20.5 |
| Magnetic Loading (T) | 0.65 | 0.65 | 0.65 | 0.65 | 0.65 |
| Bridge (mm) | 0.9 | 1.15 | 1.28 | 1.35 | 1.41 |
| Peak Mechanical Stress (MPa) | 359 | 331 | 324 | 372 | 440 |
| Safety Factor | 1.03 | 1.12 | 1.14 | 0.99 | 0.88 |

At this stage the demagnetisation of the magnet poles should be analysed at short circuit conditions using electromagnetic FEA. An example is given in fig.6. The minimum flux density value in the magnet block can be cross-checked with the material datasheet to ensure that this flux density is not beyond the knee of the demagnetisation curve at the maximum foreseeable operating temperature of the rotor. Increasing the magnet width will improve the magnets demagnetisation withstand capability. This calculation should be repeated throughout the methodology as the short circuit current value is modified.

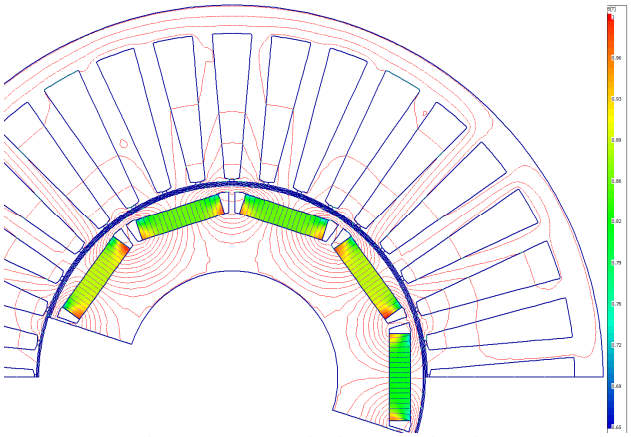

Figure 6- Demagnetisation Analysis Using FEA

### C. *Magnet Web*

The magnet web is chosen to maximise the saliency ratio as shown in fig.7. If no reasonable optimum peak is found the influence on mechanical stress and airgap flux density should also be considered. Some iteration may be required with this and the magnet length calculation in *A*.

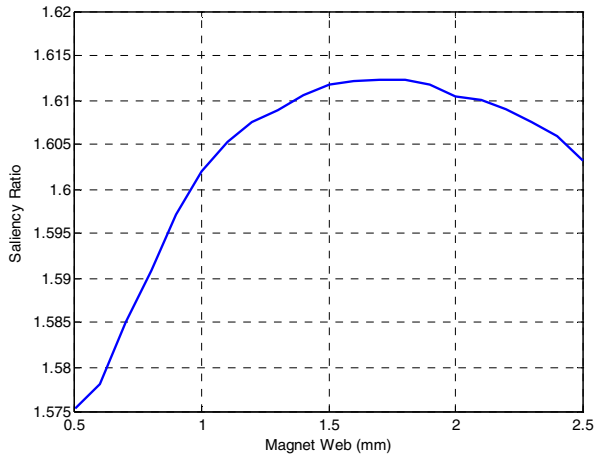


Figure 7-Variation of Saliency Ratio with Magnet Web

### D. *Projection of the Flux Guides*

Flux guides are used to guide the magnet flux through the airgap and into the stator to link the stator coils. Increasing the projection of the flux guides from the magnet block towards the rotor circumference improves the magnetic loading as more flux is directed into the airgap. However a reduced flux guide bridge depth will also increase the mechanical stress. Here the optimum projection of the flux guides that minimises the mechanical stress, for a given peak airgap flux density, is found. A number of rotors are designed with increasing flux guide projection. The distance of the magnet and flux guides arrangements from the rotor circumference is modified to solve for a magnetic loading of 0.65T. An example is given in table III; here the minimum peak mechanical stress is achieved with a flux guide projection of 0.125mm. Once the projection is chosen the distance of the designed magnet and flux guide arrangement from the airgap is then varied to achieve a specified mechanical safety factor at maximum speed. An example of a mechanical stress analysis solution is given in fig. 8.

TABLE III
FLUX GUIDE PROJECTION ANALYSIS

| *Flux Guide Projection (mm)* | *0* | *0.125* | *0.25* | *0.375* |
|---|---|---|---|---|
| Magnet Length (mm) | 20.5 | 20.5 | 20.5 | 20.5 |
| Magnetic Loading (T) | 0.65 | 0.65 | 0.65 | 0.65 |
| Flux Guide Bridge Depth (mm) | 1.56 | 1.5 | 1.43 | 1.38 |
| Magnet Inset (mm) | 2.99 | 3.05 | 3.13 | 3.20 |
| Peak Mechanical Stress (MPa) | 284 | 271 | 313 | 384 |
| Safety Factor | 1.30 | 1.37 | 1.18 | 0.96 |

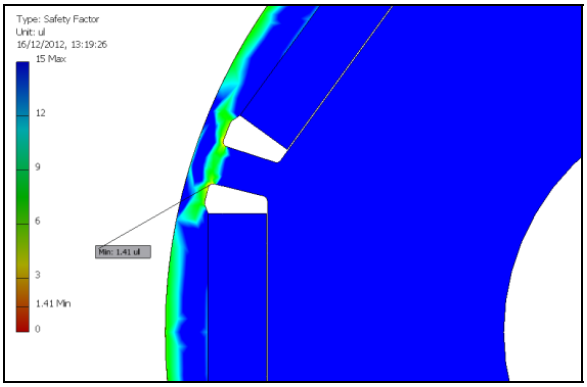


Figure 8-Mechanical Stress Analysis Solution

## V. STATOR FLUX DENSITY

The flux density in the core is an important design variable that affects iron loss, the saturation of the machine parameters as well as the slot area and hence copper loss. The flux density in the stator tooth and yoke is controlled through modification of the stator lamination dimensions. A higher tooth and yoke width gives a lower flux density and hence lower iron losses however the slot area is reduced which increases the winding resistance and hence copper loss. The chosen value of stator flux density should be close to the knee of the B-H curve for the grade of electrical steel used in the design however if the design operates at high frequencies or large peak overload torques are required then a slightly lower flux density value may be chosen. Here the optimum flux density that minimises combined copper and iron losses across the envelope is found. A number of designs with peak flux densities in the tooth and yoke ranging from 0.95T to 1.45T are created using an automated procedure. For each design the copper and iron losses are modelled and calculated from 0 to maximum speed across a torque/speed characteristic that produces rated torque (35Nm) before the base speed and rated power (20kW) after the base speed. The optimum flux density is then found where the integral of the combined copper and iron losses across the characteristic are minimised. The FEA calibrated saturation and iron loss modelling techniques described in [6] are utilised here. A rated torque and power characteristic is given in fig.9 and an example of the combined losses across this characteristic is given in fig.10.

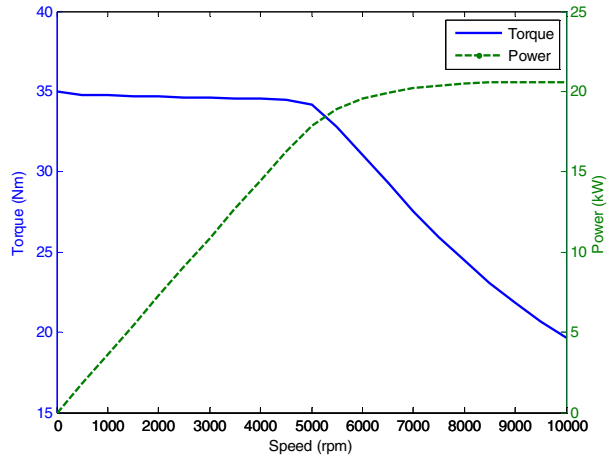


Figure 9-Rated Torque and Power Characteristic

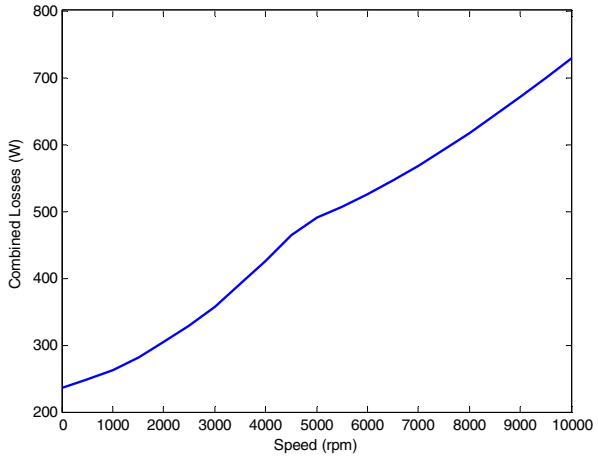


Figure 10-Combined Losses across the Rated Characteristic

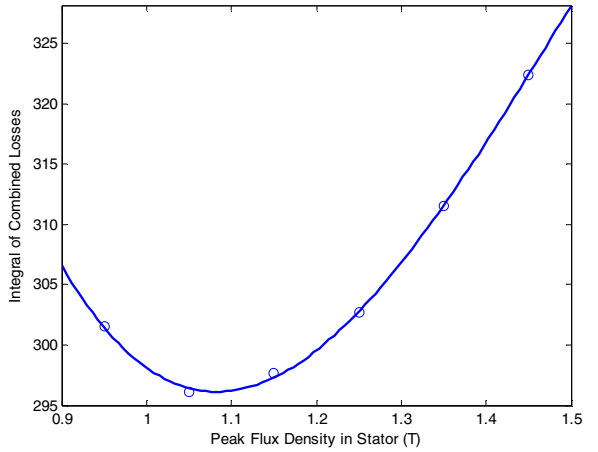


Figure 11-Integral of Combined Losses across the Rated Torque and Power Characteristic against Stator Flux Density

Fig.11 demonstrates the variation in combined losses with flux density, in this example the losses are minimised with a flux density of approximately 1.1T. Once this flux density is selected the peak torque requirement should be checked to ensure that the motor is not too heavily saturated at this working point. Some iteration will be required between this stage and the electromagnetic parameter design task.

## VI. ELECTROMAGNETIC PARAMETER DESIGN

In this task the operational envelope of the machine is optimised through modification of the active length of the machine, $l_a$, the number of turns per coil, $T_c$ and the shape of the stator teeth and slot. The affect changing these has on the performance envelope of the machine, particularly in the field weakening region, is not particularly intuitive. Here we look at each separately and consider what values optimise the motor performance, losses are considered as well as the operational envelope and then discussion is undertaken on how to choose these design variables.

In this task an element of iteration is required to deduce the optimum values. Utilising efficiency maps and torque/speed curves throughout stage V and VI with driving cycle points enables the peak efficiency region position to be optimised and the electromagnetic envelope can be designed to contain the required worst-case operating points. An example is given in fig. 12.

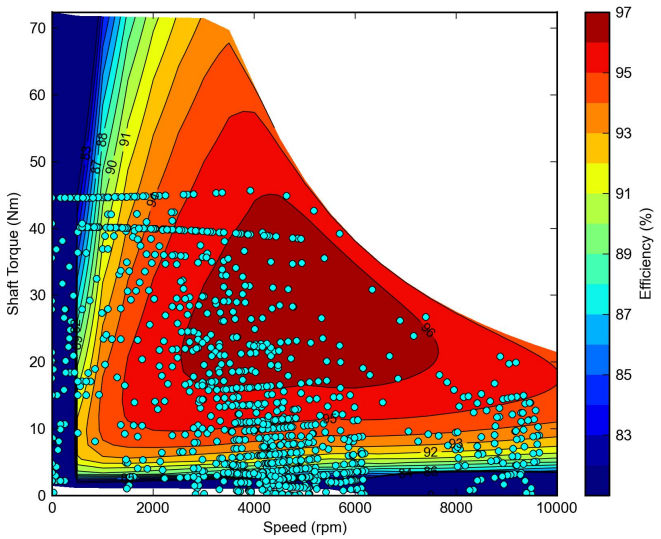


Figure 12-An Efficiency Map with Driving Cycle Points

### A. *Variation of Active Length*

The active length modifies the machine weight, the winding resistance, the permanent magnet flux linkage, $\lambda_m$ and the direct and quadrature inductances $L_d$ and $L_q$. The inductances and flux linkage scale linearly with active length therefore the short circuit current of the machine ($=\lambda_m/L_d$) is unaffected by the choice of active length.

Fig. 13 shows the torque/speed characteristics for a particular design, with various active lengths at different maximum currents. From these it can be seen how increased stack length gives improved torque/amp in the constant torque region, however, once beyond the base speed at lower currents the opposite is true, as more current is required to produce the same torque within the voltage limit. This is due to the increased d-axis current required to demagnetise the field. The peak electromagnetic output power in the field weakening region is effectively defined by the short circuit current; this is unaffected by the stack length and hence the peak electromagnetic power in the field weakening region is the same.

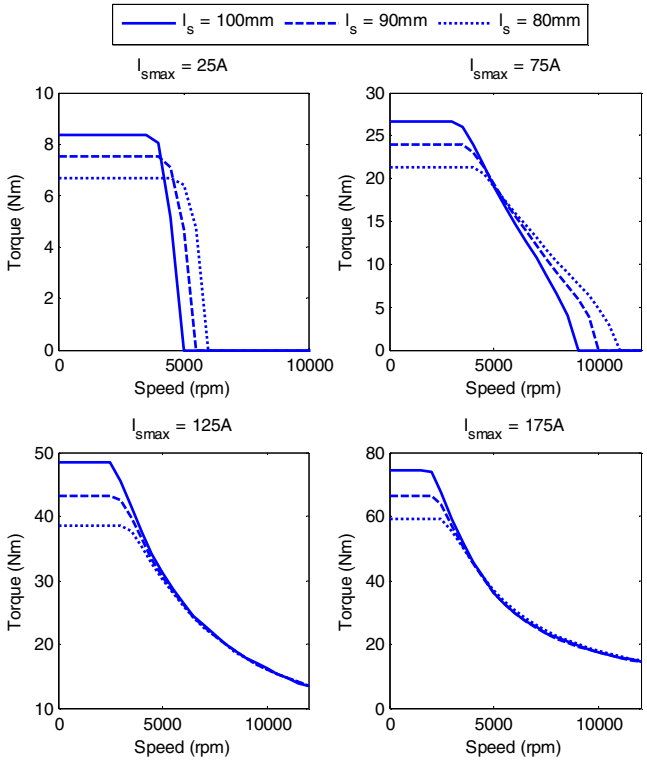


Figure 13-Influence of Active Length on Torque/Speed Characteristics

When the active length of the design is increased the winding resistance increases and the current required to achieve a particular torque in the constant torque region falls by the same ratio. As the copper loss is proportional to $I^2R$, the efficiency of the motor will be higher with a longer machine before the base speed and in addition to this the increased length will create a larger cooling surface hence the peak and continuous maximum torque at lower speeds will be improved by a longer active length. However once into field weakening the shorter machine requires less current while having a lower winding resistance and the iron loss, which becomes significant at higher speeds, will be reduced when compared to a longer and heavier machine. Therefore the stack length controls an important trade-off between high and low speed performance and should be chosen based on the required speed range and steady-state thermal performance envelope.

### *B. Number of Turns per Coil*

The number of turns per coil influences the main electromagnetic parameters $\lambda_m$, $L_d$ and $L_q$ as well as the winding resistance; $\lambda_m$ scales linearly with $T_c$ while $L_{d,q}$ is proportional to $T_c^2$. Therefore the short circuit current is also controlled by the number of turns where $I_{sc} \propto T_c/T_c^2$.

Figs. 14 and 15 show the continuous thermally constrained operating envelope for two design variations, with 2 and 3 turns per coil. This is calculated by coupling electromagnetic and thermal models to solve the maximum torque across the speed range with a steady-state winding temperature limit of 160°C. At low speeds there is very little difference between the performance of the two design variations as, although the current required to provide a given value of torque is lower for the motor with more turns, the winding resistance is increased by the same proportion that the square of the current is reduced, resulting in equal copper loss/Nm for the two designs before the base speed. It can also be seen that at higher speeds the design with a lower number of turns per coil has improved torque and power. The reason for this is that the design variant with the lower number of turns has a higher base speed, fig. 16 shows a normalised torque/amp, normalised by the difference in phase resistance, for each design against speed. This demonstrates that once into the field weakening region the motor does not operate in maximum torque/amp mode and hence the torque produced from a given amount of current falls. The difference in the two design variants performance can simply be attributed to the higher base speed for the design with a lower number of turns. The peak electromagnetically constrained peak power is also larger for the design with the lower number of turns due to the higher short circuit current. A lower number of turns appears to maximise performance however the penalty is that a higher current is required to drive the machine to achieve the same level of torque. This means a drive with a higher current rating is required which will typically cost more and the switching losses will be larger. Therefore the number of turns for the machine should be minimised while the motor is able to achieve the peak torque required from the maximum current available from the chosen drive set-up.

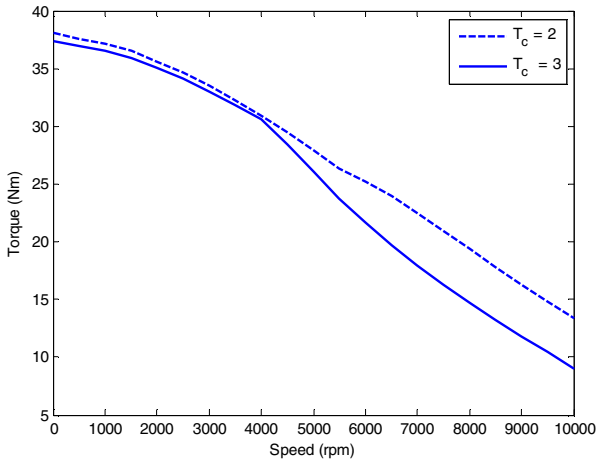


Figure 14-Thermally Constrained Continuous Maximum Torque Envelope

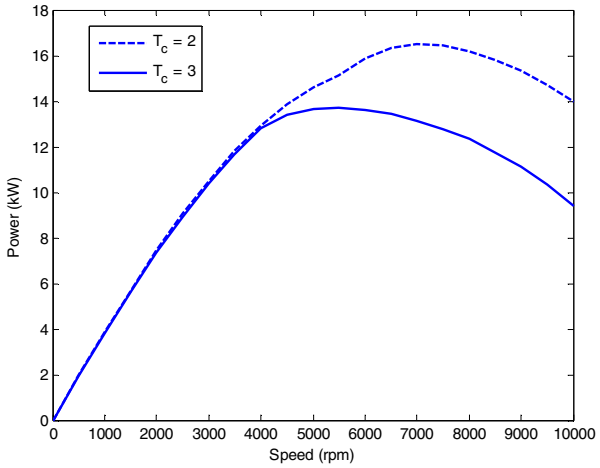


Figure 15- Thermally Constrained Continuous Maximum Power Envelope

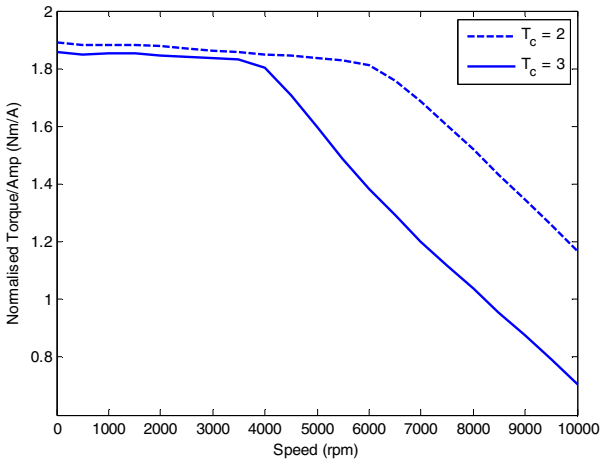


Figure 16-Normalised Torque/Amp for the Continuous Torque Envelope

### C. *Stator Tooth and Slot Optimisation*

The stator tooth and slot shapes are modified to maximise the torque production of the motor for a fixed value of copper loss. The task uses a genetic algorithm (GA) to modify the geometric parameters detailed in table IV. The electromagnetic parameters $\lambda_m$, $L_d$ and $L_q$ are evaluated using FEA. The slot area is computed based upon the geometric parameters and the winding resistance found; the phase current that produces 100W of copper loss is then calculated. Using this current value and the computed electromagnetic parameters the maximum torque at the MTPA current angle is calculated to produce a fitness value for the GA to maximise.

Table IV shows the results of the optimisation, the modification of the tooth and slot shape has increased the permanent magnet flux linkage while also slightly improving the saliency and reducing the winding resistance due to a larger slot area. This results in a 2.6% increase in the torque for the same amount of loss. The initial and optimised tooth and slot shape is shown in fig.17.

TABLE IV
RESULTS OF THE OPTIMISATION PROCEDURE

| | *Initial* | *Optimised* |
|---|---|---|
| Slot Opening (mm) | 2 | 1.005 |
| Slot Opening Angle (°) | 45 | 14.02 |
| Tooth Tip Depth (mm) | 1.5 | 0.55 |
| Radius of Slot Bottom (mm) | 0 | 0.26 |
| $L_d$ (mH) | 0.250 | 0.249 |
| $L_q$ (mH) | 0.430 | 0.431 |
| $\lambda_m$ (mWb) | 38.5 | 39.3 |
| Resistance/Phase (mΩ) | 14 | 13.8 |
| Torque (Nm) | 20.9 | 21.4 |

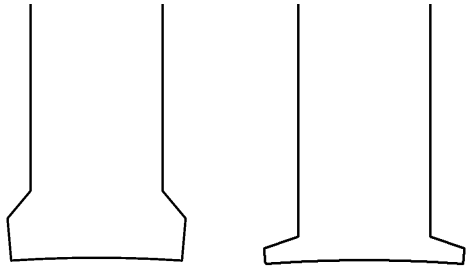

Figure 17-Initial (left) and Optimised (right) Tooth Shape

## VII. THERMAL PERFORMANCE CALCULATION

This task couples the thermal and electromagnetic modelling to compute the continuous and peak performance envelope and analyse performance across driving cycles. This allows the design engineer to evaluate cooling requirements and consider if any design changes are required. The peak (transient) and continuous (steady-state) thermal envelopes can be computed with a lumped-parameter thermal motor model. An example is given in fig. 18; here the peak envelope is defined as 60 seconds from ambient.

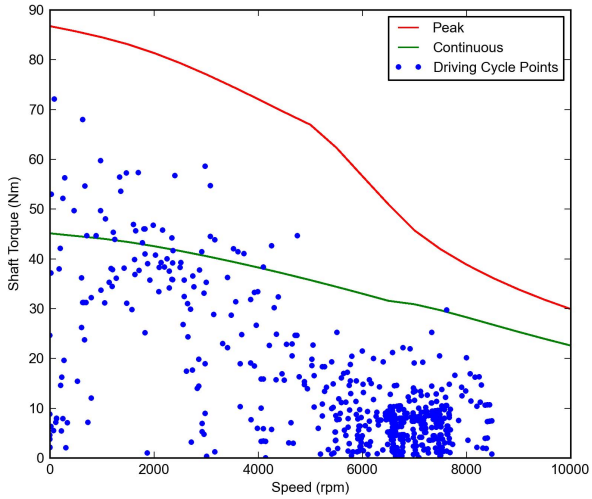


Figure 18- Peak and Continuous Thermal Envelope with Drive Cycle Points

The calculation of the losses across a worst-case driving cycle allows computation of the temperature transient across that cycle. An example is given in fig.19.

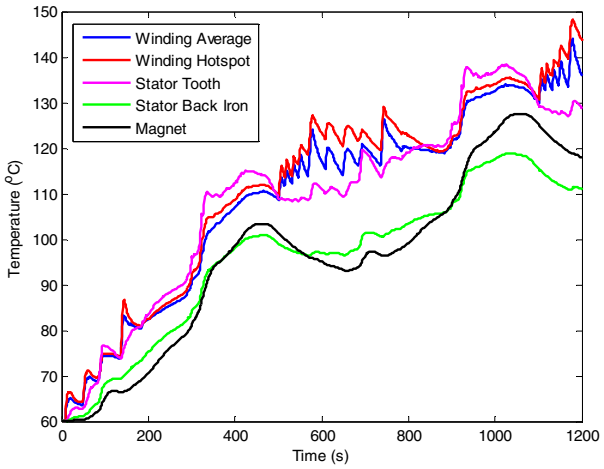


Figure 19- Example Driving Cycle Transient

From the thermal envelope and driving cycle transient calculation the cooling requirements for the design can be evaluated. If the temperature rise is too large and further improvement to the cooling system is not feasible or cost effective a number of design modifications are possible:

-Increasing the active length of the machine will improve the efficiency of the machine at low speeds as well as increasing the cooling surface area; however this will have a negative impact on the weight and cost of the design.

- Modifying the flux density in the core will control the trade-off between iron and copper loss and can be used to affect the slope of the thermally constrained torque/speed envelope.

-Increasing the outer diameter of the design will significantly improve the maximum thermally constrained peak torque as the current required to produce a given torque will reduce due to a larger rotor radius, the slot area will increase reducing the phase resistance and the active cooling surface area will increase.

## VIII. COGGING TORQUE

Cogging torque results from the interaction between the magnets on the rotor and the slotted stator. It is mainly a function of the slot/pole combination; however the magnet arrangement and stator teeth have some influence. It can be modelled using a stepping FEA computation that rotates the rotor in small increments and calculates the value of the torque at open circuit, zero winding current. The torque is calculated using the weighted stress tensor method and it is important to split the airgap into a number of layers to ensure an accurate calculation. If this is deemed excessive either the slot/pole combination should be re-considered or some modification of the tooth tip parameters such as the slot opening may reduce the magnitude.

## REFERENCES


[1] T. Finken and K. Hameyer, “Design and optimization of an IPMSM with fixed outer dimensions for application in HEVs,” in *2009 IEEE International Electric Machines and Drives Conference*, 2009, pp. 1743–1748.

[2] E. V. Kazmin, E. A. Lomonova, and J. J. H. Paulides, “Brushless traction PM machines using commercial drive technology, Part II: Comparative study of the motor configurations,” in *International Conference on Electrical Machines and Systems*, 2008.

[3] Z. Li and A. Miotto, “Concentrated-winding fractional-slot synchronous surface PM motor design based on efficiency map for in-wheel application of electric vehicle,” in *2011 IEEE Vehicle Power and Propulsion Conference*, 2011, pp. 1–8.

[4] K. I. Laskaris and A. G. Kladas, “Internal Permanent Magnet Motor Design for Electric Vehicle Drive,” *IEEE Transactions on Industrial Electronics*, vol. 57, no. 1, pp. 138–145, Jan. 2010.

[5] T. J. E. Miller, *SPEED’s Electric Machines*. 2011.

[6] J. Goss, P. H. Mellor, R. Wrobel, D. A. Staton, and M. Popescu, “The design of AC permanent magnet motors for electric vehicles: a computationally efficient model of the operational envelope,” in *6th IET International Conference on Power Electronics, Machines and Drives (PEMD 2012)*, 2012, pp. B21–B21.

[7] T. J. E. Miller and M. I. McGilp, “PC-BDC 9.1.” SPEED Laboratory, University of Glasgow, 2012. www.speedlab.co.uk

[8] Motor Design Ltd., “Motor-CAD v7.5 Software.” 2012. www.motor-design.com

[9] “Autodesk Inventor Professional.” Autodesk,Inc., 2012.

[10] Motor Design Ltd., “Motor-LAB v1.2 Software.” 2013. www.motor-design.com

[11] D. Hanselman, *Brushless Permanent Magnet Motor Design*. The Writers Collective, 2003.

[12] R. Wrobel, J. Goss, A. Mlot, and P. Mellor, “Design considerations of a brushless open-slot radial-flux PM hub motor,” in *2012 IEEE Energy Conversion Congress and Exposition (ECCE)*, 2012, pp. 3678–3685.